Linear Quadratic Regulator Design Via Metaheuristics Applied to the Damping of Low-Frequency Oscillations in Power Systems

Luis Carvalho[a], Jozias R. L. Neto[a], Jefferson C. Rezende[a], Marcus V. S. Costa[a], Elenilson V. Fortes[b,c,*], Leonardo H. Macedo[c]

[a]*Department of Engineering and Technology, Federal Rural University of the Semi-Arid Region, Rua Francisco Mota 572, Pres. Costa e Silva, 59625-900 Mossoró, RN, Brazil*

[b]*Department of Academic Areas, Goiás Federal Institute of Education, Science, and Technology, Av. Presidente Juscelino Kubitschek 775, Residencial Flamboyant, 75804-714 Jataí, GO, Brazil*

[c]*Department of Electrical Engineering, São Paulo State University, Avenida Brasil 56, Centro, 15385-000 Ilha Solteira, SP, Brazil*

Abstract

This paper proposes the application of control by state feedback using the linear quadratic regulator (LQR) optimized by metaheuristics to damp low-frequency electromechanical oscillations in electrical power systems. The current sensitivity model was used to represent the single machine infinite bus (SMIB) system in the time domain. The weighting matrices of the LQR were adjusted using four different algorithms: (i) the genetic algorithm, (ii) the differential evolution algorithm, (iii) the particle swarm optimization algorithm, and (iv) the gray wolf optimization (GWO) algorithm. In the cases considered, disturbances were applied to the electrical power system and, then, performances comparisons associated with each metaheuristic were statistically analyzed, in which the number of iterations, error, and time to achieve convergence of each algorithm were compared. From the results, it was possible to conclude that the algorithms were efficient in adjusting the weighting matrices of the LQR, providing additional damping to the poles of interest of the system. It was also possible to conclude that the GWO algorithm presented the best performance, accrediting it as a powerful tool in the study of small-signal stability for the analyzed case.

Keywords: Current sensitivity model, electric power systems, linear quadratic regulator, metaheuristics, small-signal stability.

1. Introduction

Economic growth demands the expansion and interconnection of electric power systems, which present complex structures involving the processes of generation, transmission, and distribution. Thus, stability studies of these systems aim to ensure security, reliability, and financial viability for their operation [1].

*Principal corresponding author

Email addresses: luiscarvalho9000@gmail.com (Luis Carvalho), jozias.neto@ee.ufcg.edu.br (Jozias R. L. Neto), jeffersonresende47@gmail.com (Jefferson C. Rezende), marcus.costa@ufersa.edu.br (Marcus V. S. Costa), elenilson.fortes@ifg.edu.br, elenilson.fortes@unesp.br (Elenilson V. Fortes), leohfmp@ieee.org (Leonardo H. Macedo)

These interconnections and more complex structures, observed in electric power systems, can cause electromechanical imbalances in the torque of synchronous generators and provide a favorable environment for the emergence of low-frequency electromechanical oscillations [2]. In general, these oscillations are classified as local (0.8 to 2.0 Hz) and inter-area (0.2 to 0.7 Hz) [1] and, if not properly damped, can cause the system operation to collapse. Electromechanical phenomena of this magnitude can cause changes in the oscillatory power of the transmission lines and, in more extreme events, can even cause the loss of synchronism between generation and load and, therefore, cause blackouts. The mitigation of this type of problem is still a recurring challenge in the academic and industrial environment as it can be seen in [3] and [4].

Therefore, a safe and stable operation of these systems depends, among other factors, on the damping of these oscillations by appropriate devices according to the frequency ranges in which they occur. Typically, local modes are damped using power system stabilizers (PSSs) connected to the automatic voltage regulators (AVRs) of the generators and, in the case of inter-area modes, power oscillation damping (POD) controllers, connected to flexible AC transmission system (FACTS), can be used [2].

In the literature, several models are used to represent the dynamics of power systems and can be used in small-signal stability studies: (i) the Heffron-Phillips model (HPM), which considers a simplified representation of the power system using linearized equations of the synchronous machine, was one of the first presented in the literature. However, this model has limitations, such as the need to maintain the infinite bus, as well as to reduce the power system to the terminal buses of the generators [5]; (ii) the power sensitivity model (PSM) [3], that as the HPM, is a linear model based on the nodal balance of active and reactive powers at each bus of the system; and (iii) the current sensitivity model (CSM), which is analogous to the PSM, based on the nodal current balance (Kirchhoff's current law) at each time instant and at each bus of the system [2, 6]. Both the PSM and the CSM have advantages over the HPM: there is no need to maintain the infinite bus and the transmission network is preserved. Thus, the inclusion of new devices in the power system (based on power or current injections), such as FACTS, is facilitated [2].

Three different approaches are used to adjust the parameters of the control devices in power systems, whether they are modeled using the HPM, the PSM, or the CSM. These approaches are the classic ones, robust approaches, and metaheuristic optimization algorithms [2].

The HPM has been widely used in the literature for small-signal stability studies. In [7], the authors assess the tuning of FACTS through metaheuristics such as differential evolution (DE), particle swarm optimization (PSO), whale optimization algorithm, and chaotic whale optimization algorithm. In the research developed by [8], the linear quadratic regulator (LQR) is applied for damping the low-frequency electromechanical oscillations of the SMIB system while the LQR is designed using an algebraic approach derived from the relationship between the Riccati equation and the Lagrange multipliers. Reference [9] highlights the effectiveness of the farmland fertility algorithm for tuning PSSs. In [10], a modified sine-cosine algorithm is proposed and applied to design PSSs for small-signal stability analysis.

Among the classic approaches, the residues method and the decentralized modal control [11] can be highlighted. While these approaches only consider a single static point of operation, in the robust methods, the main control objective is to stabilize the power system for a range of operational scenarios. In this context, it is possible to mention [12], which objective was to perform the simultaneous and coordinated tuning of the parameters of the supplementary damping controllers (PSSs and PODs) using the PSM and linear matrix inequalities for damping of low-frequency electromechanical oscillations in power systems.

The metaheuristic optimization algorithms have been successfully used in the literature to obtain solutions to the most diverse problems. The main advantages of the metaheuristics, when compared to the other methods mentioned above, are the speed of convergence, simplicity, and capacity to avoid local optimal solutions [13]. The genetic algorithms (GAs) and the PSO algorithm are among the most popular metaheuristic methods used to solve complex problems. The GA is based on the natural selection (evolution of the species) proposed by Charles Darwin [14]. The PSO algorithm, on the other hand, is based on the *social behavior* of many species of birds and fishes [15]. Other metaheuristics, such as the gray wolf optimization (GWO) algorithm [16], which is inspired on the hierarchical behavior of wolves, and the DE [17], which is based on evolutionary algorithms, have recently received special attention in the literature.

Several metaheuristic algorithms have been applied to the problem of tuning the parameters of PSS and POD controllers for damping low-frequency oscillations in power systems. Among the methods used to this purpose, we can highlight the artificial bee colony algorithm used in [18], the bacterial foraging optimization algorithm [19], bat algorithm [20], variable neighborhood search [2], PSO algorithm [21], and GAs [22].

For solving the discussed problem, [23] and [24] present methods based on statistical procedures. For example, [23] adopts the least-mean-squares method in the study. However, unlike optimization algorithms, they use extensive data acquisition that requires excessive computational work, making the method prone to errors when providing the parameters of the controllers. In contrast, metaheuristics use a fraction of the data to provide optimized parameters. Also, [24] adopts a stochastic approach to the control design of the LQR, which employs discrete methods for closed-loop models.

In this context, it is important to highlight the work of [25], which considers a single machine infinite bus (SMIB) system modeled using the HPM, and a DE optimization algorithm is used to parametrize the values of the state weighting matrices and the control signals of the LQR. The objective of the work is to coordinate the use of PSS and thyristor controlled series capacitor (TCSC)-POD simultaneously to stabilize the previously unstable system. The proposed method is complex due to the number of devices used and it demands a high computational effort. In addition, the work does not define the desired damping parameters for the oscillatory modes present in the power system.

Finally, [23] compares the performances of three metaheuristics: the artificial immune system, evolutionary programming, and the PSO. The main objective of the work is to optimize the synchronizing torque and damping coefficients of the SMIB system modeled using the HPM. According to the authors, the PSO presented the best results when compared to the other algorithms for obtaining the parameters. The work does not present the evaluation of the temporal response or the performance of the control actuation in the system.

Compared with the references mentioned before, this study evaluates the following concepts that have not yet been approached: (i) it develops a metaheuristic-based approach for the LQR control design applied to damping low-frequency oscillations in the SMIB system modeled with the CSM, and (ii) it performs a study involving efficient metaheuristics, i.e., GA, DE, PSO, and GWO, for the optimal control design aiming to determine which technique is more suitable for the studied problem.

Therefore, this paper proposes a novel application of metaheuristics to the design of the LQR applied to the SMIB system modeled using the CSM for closed-loop stabilization. The metaheuristics presented in this work are the GA, DE, PSO, and GWO algorithms, that are used to tune the LQR weighting matrices. The evaluation of a solution proposal of the metaheuristics is performed by analyzing the closed-loop eigenvalues of the system, including the oscillation frequency and damping coefficient, which are essential to determine the suitable conditions for stabilizing the system. Hence, the main contributions of this study are:

(i) A state feedback controller via LQR optimized using metaheuristic methods, which acts on the AVR stabilization and is applied to the SMIB system modeled using the CSM. This proposal presents a control technique that guarantees the stability of the system with a simpler configuration in comparison to the proposal of [25], which considers the coordination of the PSS and the TCSC using LQR. As it was already mentioned, there are several advantages of representing electric power systems using the CSM instead of the HPM;

(ii) Optimal control guarantee based on the quadratic performance index via LQR tuned by metaheuristics. The proposed method considers the desired eigenvalues as the evaluation function of the metaheuristics, different from [25], which does not present a minimum damping requirement. Therefore, the proposed control strategy allows to combine the principles of optimal control with the desired parameters and the effectiveness of the metaheuristics for solving complex problems;

(iii) An approach that allows determining the desired damping range. Differently from [23] and [25], which do not define a desired damping for the solutions, in the present work, a minimum desired damping for the poles of interest is considered;

(iv) To implement the GA, DE, PSO, and GWO optimization algorithms to perform comparative performances analysis with the SMIB system modeled using the CSM. The performances of the algorithms are evaluated using statistical methods that demonstrate that the GWO algorithm is the most efficient algorithm to stabilize the plant under study using the LQR, even better than the DE algorithm proposed by [25].

It should be highlighted that regarding point (i), the SMIB system modeled using the CSM is an original contribution of this paper. Moreover, as mentioned in point (ii) the proposed approach ensures a minimum damping level for the system, differently from other works, such as [23] and [25], that only find a stable solution for the problem. Note that the solutions found by the approach presented in this article will be more effective than the ones found in existing approaches available in the literature, such as the ones presented by [23] and [25]. The desired damping range mentioned in point (iii) will allow the effectiveness of the solution. Finally, as mentioned in point (iv) we show that the GWO algorithm presents better performance to solve this problem than other traditional metaheuristics that were used for the same purpose.

Thus, the GWO metaheuristic can be accredited as a powerful technique for the LQR control design applied to power systems. It is also worth noting that none of the statistical approaches used in this work (number of iterations, error, and time of convergence) is used in the works aforementioned.

The main advantages of the approach presented in this study are: (i) when adequately designed, the LQR guarantees the optimal closed-loop performance; (ii) the use of metaheuristic algorithms applied to the LQR design enhances the results of the control strategy; (iii) the presented metaheuristic-based LQR design applied to the SMIB system closed-loop stabilization ensures better performance combined with the desired poles specification; and (iv) the proposed study performs a complete analysis of the performances of the metaheuristics and evaluates their suitability for the SMIB system stabilization. Thus, the arguments presented evidence that the method employed to solve the SMIB system stabilization is innovative. Differently from previous works, the results are supported with statistical analysis for the LQR optimal control design.

The organization of the work is as follows: Section 2 describes the modeling of the SMIB system in the state space using the CSM; Section 3 defines the control strategy used to stabilize the system; Section 4 presents and discusses the metaheuristics used in this work; Section 5 presents further details of the implementation of the metaheuristics; Section 6 presents the tests and results; finally, Section 7 presents the conclusions and future works.

2. The Current Sensitivity Model for the Single Machine Infinite Bus System

The SMIB is a classic system used in the literature for the study of electric power systems stability [1]. Fig. 1 illustrates its single-line diagram, which consists of a synchronous generator, a load, a transmission line, and an infinite bus.

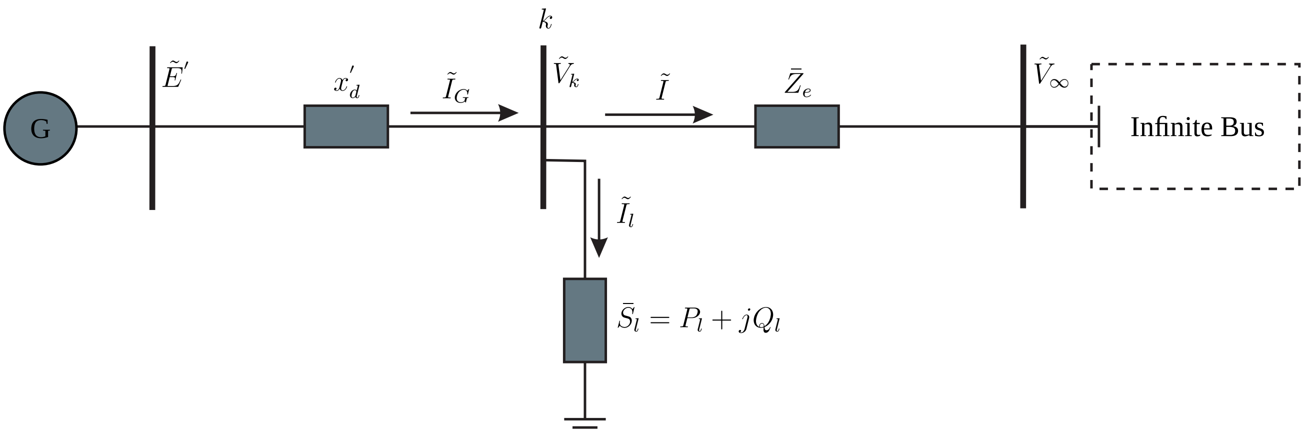

Figure 1: Single machine infinite bus system.

In Fig. 1, $\tilde{E}'$ and $\tilde{V}_k$ are phasors representing, respectively, the internal and terminal voltages of the synchronous generator. $\tilde{V}_\infty$ is the voltage phasor at the infinite bus, $\tilde{I}_G$ is the current phasor supplied by the generator, and x'_d its direct axis transient reactance. $\tilde{I}_L$ is the current phasor absorbed by the load $P_l + jQ_l$, and $\tilde{I}$ is the current phasor through the transmission line with impedance $\bar{Z}_e$.

By analyzing Fig. 1, by inspection, it is possible to obtain (1) $-$ (4).

$$V_d = V_k \sin(\delta - \theta) \tag{1}$$

$$V_q = V_k \cos(\delta - \theta) \tag{2}$$

$$I_d = \frac{E'_q - V_q}{x'_d} \tag{3}$$

$$I_q = \frac{V_q}{x_q} \tag{4}$$

In (1) $-$ (4), the indices d and q are related to the rotating coordinate system (d, q) of the generator G, x_q and δ are, respectively, the synchronous reactance of the quadrature axis and the internal angle of the generator G and θ is the voltage angle at the terminal bus k. Finally, E'_q, V_q, and V_d are, respectively, the quadrature axis internal voltage, the terminal voltage in phase and in quadrature of generator G [26].

2.1. Currents Generated by the Synchronous Generator

According to [26], it is possible to use Park's transformation in (3) and (4), being possible to migrate the quantities from the coordinate system (d, q) to the coordinates (r, m). By inspection, it is possible to obtain (5) and (6).

$$I_{G_r} = \sin(\delta)\left(\frac{E'_q - V_q}{x'_d}\right) + \cos(\delta)\left(\frac{V_d}{x_q}\right) \tag{5}$$

$$I_{G_m} = -\cos(\delta)\left(\frac{E'_q - V_q}{x'_d}\right) + \sin(\delta)\left(\frac{V_d}{x_q}\right) \tag{6}$$

Equations (5) and (6) represent the real (I_{G_r}) and imaginary (I_{G_m}) components of the currents generated by the synchronous machine of the SMIB system.

2.2. Current on the Transmission Line

By considering $\bar{Z}_e = r_e + jx_e$ and $\tilde{V}_k = V_k \cos(\theta) + jV_k \sin(\theta)$ in Fig. 1, it is possible to calculate the current phasor, $\tilde{I}$, on the line between the terminal bus k and the infinite bus of the SMIB system, as presented in (7) and (8).

$$I_r = \frac{r_e\left[V_k \cos(\theta) - V_\infty\right] + x_e V_k \sin(\theta)}{Z_e^2} \tag{7}$$

$$I_m = \frac{r_e V_k \sin(\theta) - x_e\left[V_k \cos(\theta) - V_\infty\right]}{Z_e^2} \tag{8}$$

In (7) and (8), I_r and I_m represent the real and imaginary components of the currents on the transmission line of the SMIB system, respectively.

2.3. Load Current

Suppose there is a load connected to the terminal bus of the generator (see Fig. 1). Also, suppose that the complex power of this load is $\bar{S}_l = P_l + jQ_l$. Thus, it is possible, by inspection, to calculate the current demanded by this eventual load, $\tilde{I}_l$, as shown in (9) and (10).

$$I_{l_r} = \frac{P_l \cos(\theta) + Q_l \sin(\theta)}{V_k} \tag{9}$$

$$I_{l_m} = -\frac{Q_l \cos(\theta) - P_l \sin(\theta)}{V_k} \tag{10}$$

Equations (9) and (10) represent the real and imaginary components of the load currents of the SMIB system, respectively.

2.4. Nodal Current Balance

Differently from the classic models available in the literature, particularly the HPM [1], the CSM is based on the application of the nodal current balance at each bus of the power system. In this particular case, the balance is considered at the terminal bus of the generator of the SMIB system. Mathematically, this balance is represented by (11) and (12).

$$\tilde{I}_{G_r} - \tilde{I}_r - \tilde{I}_{l_r} = 0 \tag{11}$$

$$\tilde{I}_{G_m} - \tilde{I}_m - \tilde{I}_{l_m} = 0 \tag{12}$$

Equations (11) and (12) are algebraic equations that represent the balance of the real and imaginary components of the currents at the terminal bus of the generator of the SMIB system.

2.5. Differential Equations of the CSM

To finalize the representation of power system using the CSM, it is necessary to incorporate the differential equations that represent the dynamics of the synchronous machine, presented below.

2.5.1. Internal Voltage of the Synchronous Machine

As presented in [26], the variation of the internal voltage of the synchronous machine is expressed by (13).

$$\dot{E}'_q = \frac{1}{T'_{d_0}} \left[E_{\text{fd}} - \frac{x_d}{x'_d} E'_q + \left(\frac{x_d}{x'_d} - 1 \right) V_k \cos(\delta - \theta) \right] \tag{13}$$

In (13), T'_{d_0} is the transient time constant of direct axis in open circuit, E_{fd} is the excitation voltage of the synchronous machine and x_d is the direct axis transient synchronous reactance of the generator of the SMIB system.

2.5.2. Field Voltage of the Synchronous Machine

The effects of the field winding of the synchronous machine are considered when the synchronous generator is equipped with an AVR [26], as presented in Fig. 2.

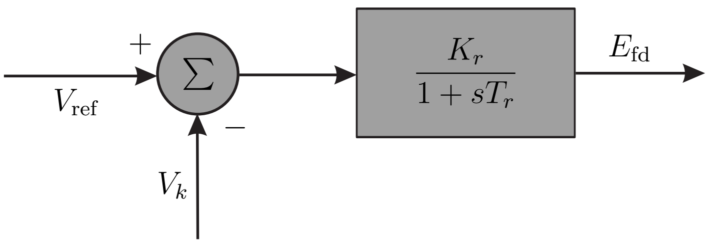

Figure 2: Block diagram of the AVR.

By inspection, based on Fig. 2, it is possible to obtain (14).

$$\dot{E}_{\text{fd}} = -\frac{1}{T_r}E_{\text{fd}} + \frac{K_r}{T_r}V_{\text{ref}} - \frac{K_r}{T_r}V_k \tag{14}$$

In (14), K_r and T_r are, respectively, the gain and the time constant of the AVR and V_{ref} is the reference voltage of the generator.

2.5.3. *Electromechanical Equations of the Synchronous Machine*

According with [27], the mechanical quantities of the synchronous machine, the angular speed of the rotor (ω) and its internal angle (δ) are presented in (15) and (16).

$$\dot{\omega} = \frac{1}{M}(P_m - P_G - D\omega) \tag{15}$$

$$\dot{\delta} = \omega_0\omega \tag{16}$$

In (15) and (16), $M = 2H$ and represents the inertia constant, P_m is the input mechanical power, P_G is the active power generated by the synchronous machine, D is the damping torque coefficient of the electromechanical loop, and $\omega_0 = 377$ rad/s.

2.6. *Representation of the SMIB System using the CSM in the Time Domain*

As already mentioned, the CSM is based on Kirchhoff's current law at the nodes and its application provides the algebraic equations of the model [6]. The electric power systems modeled using the CSM can be expressed by (17) $-$ (20).

$$\begin{bmatrix} \Delta\dot{\mathbf{x}} \\ \mathbf{0} \end{bmatrix} = \begin{bmatrix} \mathbf{J}1 & \mathbf{J}2 \\ \mathbf{J}3 & \mathbf{J}4 \end{bmatrix} \begin{bmatrix} \Delta\mathbf{x} \\ \Delta\mathbf{z} \end{bmatrix} + \begin{bmatrix} \mathbf{B}1 \\ \mathbf{B}2 \end{bmatrix} \begin{bmatrix} \Delta\mathbf{u} \end{bmatrix} \tag{17}$$

$$\Delta\mathbf{x} = \begin{bmatrix} \Delta\omega & \Delta\delta & \Delta E'_q & \Delta E_{\text{fd}} \end{bmatrix}^T \tag{18}$$

$$\Delta\mathbf{u} = \begin{bmatrix} \Delta P_m & \Delta V_{\text{ref}} & \Delta P_l & \Delta Q_l \end{bmatrix}^T \tag{19}$$

$$\Delta\mathbf{z} = \begin{bmatrix} \Delta\theta & \Delta V_k \end{bmatrix}^T \tag{20}$$

The sub-matrices $\mathbf{J}1$, $\mathbf{J}2$, $\mathbf{J}3$, and $\mathbf{J}4$ shown in (17) are detailed in (21) and (22). In (18), $\Delta\mathbf{x}$ represents the state variables of the system, while $\Delta\omega$, $\Delta\delta$, $\Delta E'_q$, and ΔE_{fd} represent, respectively, the angular speed of the rotor, the internal angle of the rotor, the internal quadrature voltage, and the field voltage of the synchronous generator.

In (19), $\Delta\mathbf{u}$ represents the input vector of the system, in which ΔP_M is the input mechanical power, ΔV_{ref} is the reference voltage of the AVR, and ΔP_l and ΔQ_l represent, respectively, the active and reactive power drained by the load $P_l + jQ_l$ connected to bus k.

Finally, (20) presents the algebraic variables of the system. These are represented by $\Delta\theta_k$ and ΔV_k, which correspond, respectively, to the voltage phase angle and the voltage magnitude at bus k.

$$\mathbf{J}1 = \begin{bmatrix} -\frac{D}{M} & -\frac{K1}{M} & -\frac{K2}{M} & 0 \\ \omega_0 & 0 & 0 & 0 \\ 0 & -\frac{KA}{T'_{d0}} & -\frac{x_d}{x'_d T'_{d0}} & \frac{1}{T'_{d0}} \\ 0 & 0 & 0 & -\frac{1}{T_r} \end{bmatrix}, \ \mathbf{J}2 = \begin{bmatrix} -\frac{K1}{M} & -\frac{K3}{M} \\ 0 & 0 \\ \frac{KA}{T'_{d0}} & \frac{KV}{T'_{d0}} \\ 0 & -\frac{K_r}{T_r} \end{bmatrix} \tag{21}$$

$$\mathbf{J}3 = \begin{bmatrix} 0 & R2_G & R1_G & 0 \\ 0 & M2_G & M1_G & 0 \end{bmatrix}, \ \mathbf{J}4 = \begin{bmatrix} A_r & B_r \\ A_m & B_m \end{bmatrix} \tag{22}$$

$$\mathbf{B}1 = \begin{bmatrix} \frac{1}{M} & 0 & 0 & 0 \\ 0 & 0 & 0 & 0 \\ 0 & 0 & 0 & 0 \\ 0 & \frac{K_r}{T_r} & 0 & 0 \end{bmatrix}, \ \mathbf{B}2 = \begin{bmatrix} 0 & 0 & -C3_r & -C4_r \\ 0 & 0 & -C3_m & -C4_m \end{bmatrix} \tag{23}$$

From the above, the power system model represented using the CSM in the state space can be rewritten according to (24).

$$\Delta\dot{\mathbf{x}} = \mathbf{A}\Delta\mathbf{x} + \mathbf{B}\Delta\mathbf{u} \tag{24}$$

In (24), $\mathbf{A} = \mathbf{J}1 - \mathbf{J}2\mathbf{J}4^{-1}\mathbf{J}3$ is the state matrix and $\mathbf{B} = \mathbf{B}1 - \mathbf{J}2\mathbf{J}4^{-1}\mathbf{B}2$ is the input matrix of the system. More details about the formulation and the coefficients shown in the (17) $-$ (23) can be found in Appendix A.

3. Control Strategy

According to [28], the optimal LQR consists of a systematic method that minimizes the quadratic performance index, as presented in (25).

$$J(\Delta\mathbf{x}, \mathbf{u}_{\text{Vs}}, t) := \int_0^{\infty} \left[\Delta\mathbf{x}(t)^T \mathbf{Q}_c \Delta\mathbf{x}(t) + \mathbf{u}_{\text{Vs}}^T(t)\mathbf{R}_c\mathbf{u}_{\text{Vs}}(t)_{\text{Vs}}\right] dt \tag{25}$$

According to [6], the model in the state space of the SMIB system using the CSM, expressed in (24), can be re-adapted to consider a supplementary voltage vector of the AVRs coupled to the generators and, thus, (26) can be obtained.

$$\Delta\dot{\mathbf{x}} = \mathbf{A}\Delta\mathbf{x} + \mathbf{B}_{\mathrm{Vs}}\mathbf{u}_{\mathrm{Vs}} + \mathbf{B}\Delta\mathbf{u} \tag{26}$$

In (26), $\mathbf{u}_{\mathrm{Vs}} = -K_{\mathrm{LQR}}\Delta\mathbf{x}$, $\mathbf{B}_{\mathrm{Vs}} = [0 \;\; 0 \;\; 0 \;\; \frac{K_r}{T_r}]^T$, in which K_r and T_r are, respectively, the gain and the time constant of the AVR. In addition, $K_{\mathrm{LQR}} = \mathbf{R}_c^{-1}\mathbf{B}_{\mathrm{Vs}}^T\mathbf{N}$ is the state space feedback gain, in which $\mathbf{N} = \mathbf{N}^T \succeq 0$ is symmetric positive semi-definite, and can be obtained from the solution of the infinite horizon problem, given by Riccati equation (27).

$$\mathbf{A}^T\mathbf{N} + \mathbf{N}\mathbf{A} - \mathbf{N}\mathbf{B}_{\mathrm{Vs}}\mathbf{R}_c^{-1}\mathbf{B}_{\mathrm{Vs}}^T\mathbf{N} + \mathbf{Q}_c = 0 \tag{27}$$

In (27), $\mathbf{Q}_c \succeq 0$ and $\mathbf{R}_c \succ 0$ are the weighting matrices of the states and the control signal, respectively.

The state-space diagram of the AVR, based on the control law presented in this section, is illustrated in Fig. 3. In this work, the weighting matrices of the LQR, $\mathbf{Q}_c$ and $\mathbf{R}_c$, are obtained from four metaheuristics, which are discussed below in Section 4. For the studied problem, it was verified that a diagonal matrix $\mathbf{Q}_c$ is sufficient for obtaining the desired damping values. Nonetheless, it is possible to apply the proposed approach considering a symmetric and full $\mathbf{Q}_c$ matrix.

4. Techniques to Adjust the Parameters of the LQR Controller

An efficient approach for solving optimization problems, which does not necessarily require an explicit mathematical formulation of the problem, is to use a metaheuristic [29].

Some metaheuristic methods are inspired by natural phenomena, and use operators based on physical, biological, or behavioral phenomena to solve complex optimization problems. These methods can be classified into four main groups: algorithms based on (i) natural evolution, (ii) physical phenomena, (iii) swarm, and (iv) human behavior [30]. In general, it is possible to observe in the literature that algorithms based on the natural evolution and in the social behavior of certain individuals in nature are the most used to obtain solutions of power systems optimization problems. These two categories are illustrated in Fig. 4.

The evolutionary algorithms are based on Darwin's principle of evolution of the species, and use specific operators in order to select, over successive generations, the fittest individuals to originate the next generation. According to [31] the main algorithms covered in this subcategory are the GA and the DE algorithm. On the other hand, the PSO and the GWO are the main algorithms in the swarm-based category that use techniques that mimic the individual and social behavior of certain animals found in nature.

4.1. Genetic Algorithms

The GA is a population-based optimization tool originally developed using mechanisms from Darwin's evolutionary theory. It was first suggested in the 1970s by Holland [14] and can be seen as a class of evolutionary algorithms [29].

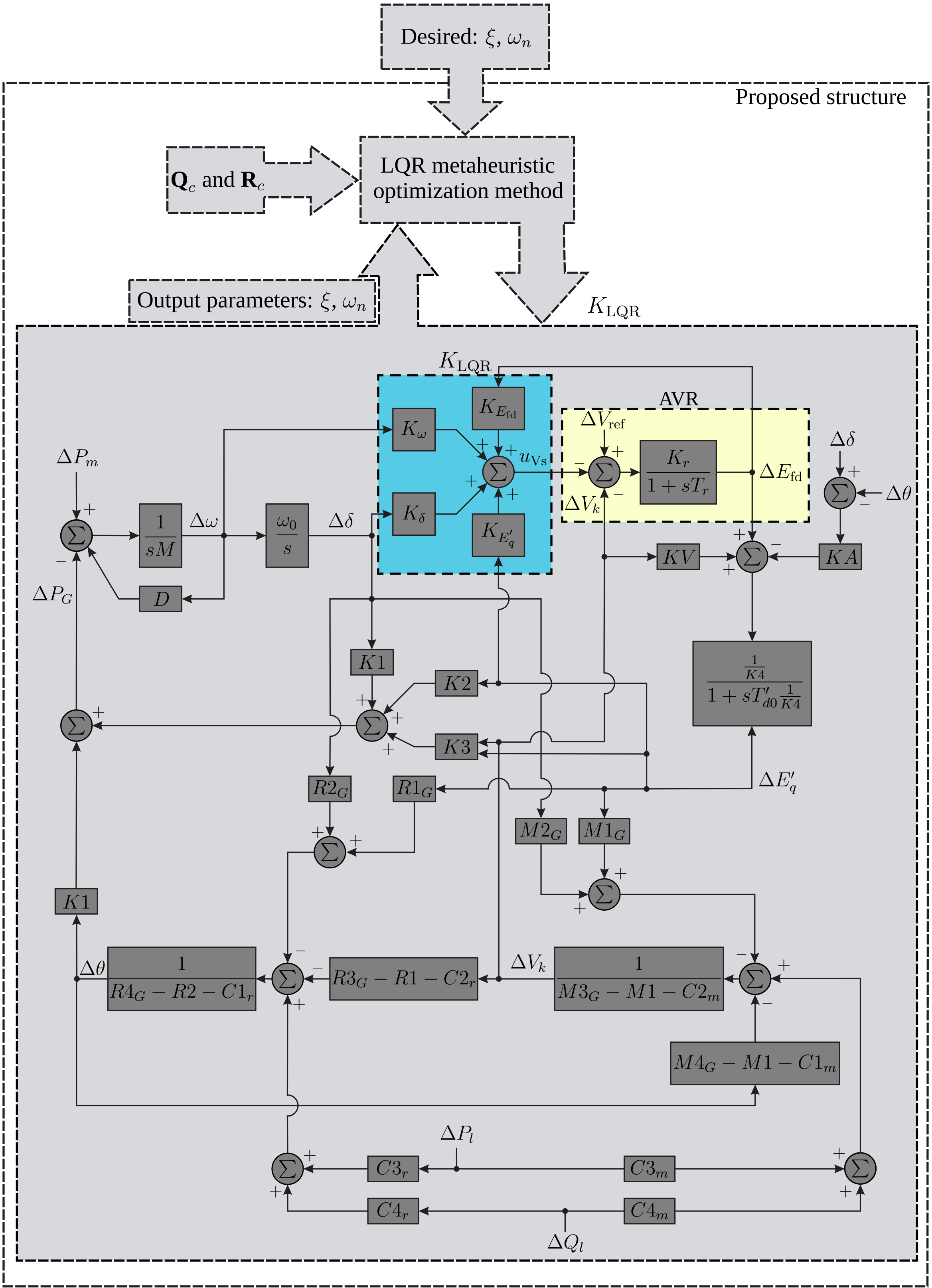

Figure 3: Block diagram representation of the state space equations of the AVR.

Initially, the parameters t_{cro}, t_{mut}, and $g_{\max}$, which represent, respectively, the crossover probability, mutation probability, and maximum number of generations, are defined. For the problem discussed in this work, the individuals that represent a solution proposal are the diagonal values of the LQR weighting matrices ($\text{diag}(\mathbf{Q}_c)$, $\mathbf{R}_c$, respectively) necessary to obtain the feedback gain K_{LQR}, as illustrated in Fig. 7, and explained in Section 5. The fitness function is obtained using the CSM, and includes the

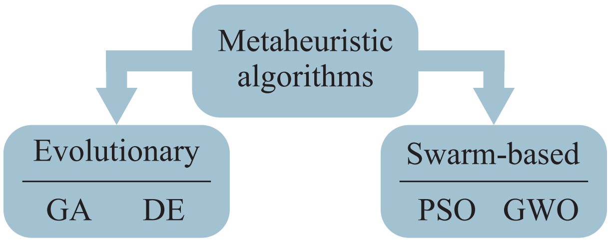

Figure 4: Categories of metaheuristic algorithms.

frequency of oscillation (ω_n) and the damping (ξ_i) of the poles of interest of the power system.

At each iteration of the GA, a new population is generated based on the individuals of the current population. The solutions of the new population are obtained by applying a sequence of operators, i.e., the selection, crossover, and mutation. The proportional selection operator using a roulette wheel, that gives more chance to the fittest solutions to be chosen to go through the crossover operator, is used in this work. The single-point crossover is applied to each pair of solutions provided by the selection operator, and exchange the parts of the solutions separated by a point randomly chosen. The mutation slightly changes the value of a variable considering its bounds. After the new population is formed, the fitness of each individual is evaluated. Finally, the elitism operator is applied: the best solution of the current population replaces the worst solution of the new population. The steps of the GA are presented in Algorithm 1.

Algorithm 1: Genetic Algorithm

```
Initialization.
while g ≤ g_max do
    for each individual do
        Apply the proportional selection operator using the roulette wheel.
        if rand[0, 1] ≤ t_cro then
            Apply the single-point crossover operator.
        end
        if rand[0, 1] ≤ t_mut then
            Apply the mutation operator.
        end
        Apply the elitism operator.
    end
    Update the population. Evaluate the fitness function of each individual;
    g ← g + 1.
end
```

4.2. *Differential Evolution*

Analogously to the GA, the DE algorithm is a population-based search method. It considers a population of n_p individuals that form each generation, i.e., $\mathbf{y}_i^g$, with $i = 1, 2, 3, \cdots, n_p$, where i is the number of the individual generated at each generation g [17].

Fig. 5 illustrates the procedure used in the mutation operator of the DE algorithm. It consists of performing a weighted difference between two individuals of the current population ($\mathbf{y}_{r2}^g - \mathbf{y}_{r3}^g$) for generating a third individual (28), in which F is a scalar number.

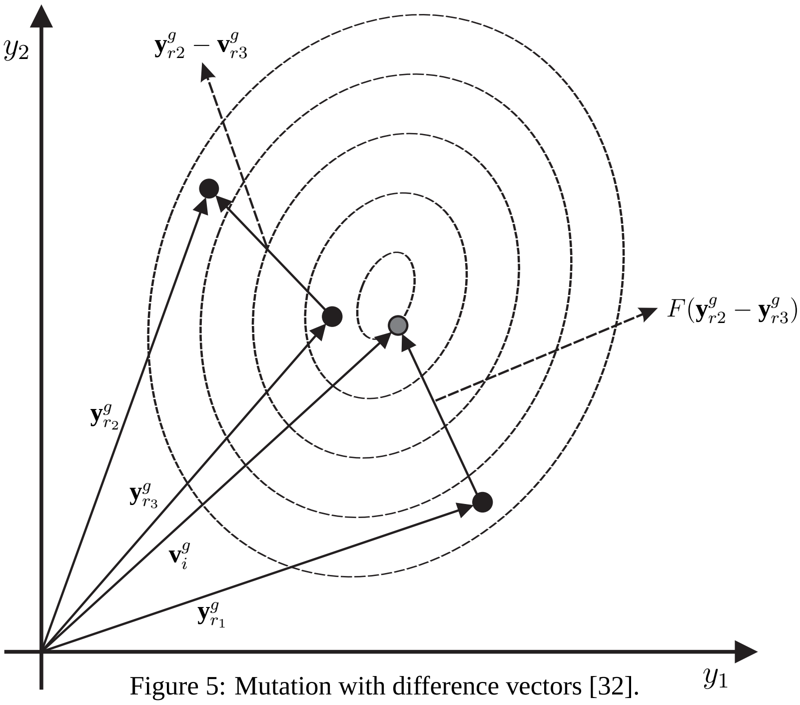

Figure 5: Mutation with difference vectors [32].

$$\mathbf{v}_i^g = \mathbf{y}_{r1}^g + F \cdot (\mathbf{y}_{r2}^g - \mathbf{y}_{r3}^g) \tag{28}$$

After the differential mutation and the binomial crossover procedure (in which each position of the individual $\mathbf{y}_i^g$ is replaced by a position of the vector $\mathbf{v}_i^g$ with a crossover probability), the following step is the calculation of the fitness function of the resulting individual, $f(\mathbf{u}_i^g)$, and the comparison with the fitness function of the current individual $f(\mathbf{y}_i^g)$. The individual with the lowest cost participates in the new generation. This process is repeated until the stopping criteria is met. More details about the DE algorithm can be found in [17, 33] and Algorithm 2.

Algorithm 2: Differential Evolution

Initialization.
while $g \leq g_{\max}$ **do**
    for *each individual* **do**
        Apply the differential mutation operator;
        Apply the binomial crossover operator with $\mathbf{y}_i^g$ and $\mathbf{v}_i^g$;
        Evaluate the new individual $\mathbf{u}_i^g$.
        if $f(\mathbf{u}_i^g) < f(\mathbf{y}_i^g)$ **then**
            Replace the current individual.
        else
            Maintain the current individual.
        end
    end
    Update the population;
    $g \leftarrow g + 1$.
end

4.3. *Particle Swarm Optimization*

According to [15], the PSO algorithm consists of a metaheuristic idealized based on the *social behavior* of certain individuals found in nature, for example, birds and fishes, associating the experience of individual and group behavior of a given flock or swarm.

This metaheuristic uses a set of n_p particles with their positions $\mathbf{y}_i^g$, in which i represents the index of the particle in the swarm and g is the iteration, that form a swarm in motion looking for the best solution for an optimization problem.

The combination of individual experiences is used to adjust the exploration procedure of this heuristic. The swarm is driven by the velocities $\mathbf{v}_i^g$, updated at the g^{th} iteration of the algorithm using (29) and (30).

$$\mathbf{v}_i^{g+1} = C_0\mathbf{v}_i^g + C_1\mathbf{r}_{1,i}^g \odot (\mathbf{y}_i^{\text{best},g} - \mathbf{y}_i^g) + C_2\mathbf{r}_{2,i}^g \odot (\mathbf{h}^{\text{best},g} - \mathbf{y}_i^g) \tag{29}$$

$$\mathbf{y}_i^{g+1} = \mathbf{y}_i^g + \mathbf{v}_i^{g+1} \tag{30}$$

In (29) and (30), C_0, C_1, and C_2 are, respectively, the inertia factor, cognitive factor, and social factor of each swarm, $\mathbf{r}_{1,i}^g$ and $\mathbf{r}_{2,i}^g$ are vectors with random values evenly distributed in the interval $[0,\ 1]$, $\mathbf{y}_i^{\text{best},g}$ and $\mathbf{h}^{\text{best},g}$ are, respectively, the best position of particle i found so far and the global best position found for a particle [34]. The operator $\odot$ is the Hadamard product (element-wise multiplication). Algorithm 3 shows the steps of the PSO algorithm.

Algorithm 3: Particle Swarm Optimization Algorithm

Initialization.
while $g \leq g_{\max}$ **do**
  for *each particle* **do**
    Evaluate the swarm and determine $\mathbf{y}_i^{\text{best},g}$ and $\mathbf{h}^{\text{best},g}$;
    Calculate the velocity of the particle in the swarm using (29);
    Update the position of the particle in the swarm using (30).
  end
  Update the swarm;
  Calculate the evaluation function for each particle;
  $g \leftarrow g + 1$.
end

4.4. *Gray Wolf Optimization Algorithm*

The GWO algorithm is based on the hierarchical social behavior of a wolf pack. This hierarchy is divided into four levels without gender restriction, as illustrated in Fig. 6. At the top of the hierarchy is the alpha (α), which leads the pack. Below in the hierarchy are the betas (β), which have the function of assisting the alpha in making decisions in the leadership of the pack and, thus, are the immediately most likely candidates to become an alpha. Next, we can find the deltas (δ), which are submitted to commands and have the function of assisting alpha and betas. At the end of the hierarchy, the omegas (ω) stand out, which are submitted to the decisions of the superiors in the hierarchy [16].

In the GWO algorithm, the hunting skills of wolves are addressed in the implementation of the optimization technique. The hunting is carried out in such a way that the best solution to the problem

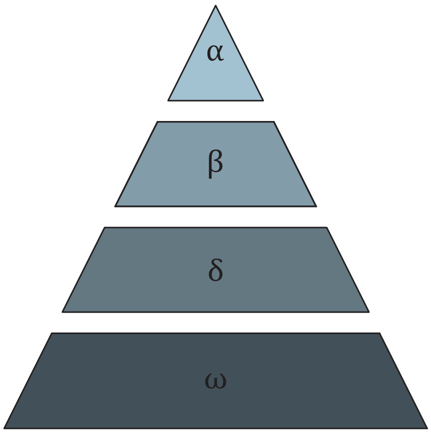

Figure 6: Hierarchy of the GWO algorithm [16].

is surrounded, tracked, and captured. The equations that illustrate this approach to the wolf pack are presented in (31) and (32).

$$\mathbf{d}_i^g = |\mathbf{c}_i^g \odot \mathbf{y}_p^g - \mathbf{y}_i^g| \tag{31}$$

$$\mathbf{y}_i^{g+1} = \mathbf{y}_p^g - \mathbf{a}_i^g \odot \mathbf{d}_i^g \tag{32}$$

In (31) and (32), g is the current iteration and i is the current wolf, $\mathbf{y}_p^g$ is the position of the best solution or prey, and $\mathbf{y}_i^g$ is the position of a wolf. The operator $|.|$ provides the absolute value of each element of a vector. Furthermore, the vectors $\mathbf{a}_i^g$ and $\mathbf{c}_i^g$ are calculated using (33) and (34).

$$\mathbf{a}_i^g = 2 \cdot \mathbf{w}_i^g \odot \mathbf{r}_{1,i}^g - \mathbf{w}_i^g \tag{33}$$

$$\mathbf{c}_i^g = 2 \cdot \mathbf{r}_{2,i}^g \tag{34}$$

In (33) and (34), the components of the vector $\mathbf{w}_i^g$ are linearly decreasing values obtained from the interval $[0, 2]$ and are adjusted during the iterations. In addition, $\mathbf{r}_{1,i}^g$ and $\mathbf{r}_{2,i}^g$ are vectors randomly generated in the interval $[0, 1]$.

In the next stage, the alpha leads the hunt with the betas and deltas, since they are the ones that possibly have the closest proximity to the prey. In this step, the locations of the individuals from the top three levels of the hierarchy, including the omegas, update the positions of the individuals. The equations that represents this step can be verified in the (35) $-$ (41).

$$\mathbf{d}_{\alpha,i}^g = |\mathbf{c}_{1,i}^g \odot \mathbf{y}_\alpha^g - \mathbf{y}_i^g| \tag{35}$$

$$\mathbf{d}_{\beta,i}^g = |\mathbf{c}_{2,i}^g \odot \mathbf{y}_\beta^g - \mathbf{y}_i^g| \tag{36}$$

$$\mathbf{d}_{\delta,i}^g = |\mathbf{c}_{3,i}^g \odot \mathbf{y}_\delta^g - \mathbf{y}_i^g| \tag{37}$$

$$\mathbf{y}_{1,i}^g = \mathbf{y}_\alpha^g - \mathbf{a}_{1,i}^g \odot \mathbf{d}_{\alpha,i}^g \tag{38}$$

$$\mathbf{y}_{2,i}^g = \mathbf{y}_\beta^g - \mathbf{a}_{2,i}^g \odot \mathbf{d}_{\beta,i}^g \tag{39}$$

$$\mathbf{y}_{3,i}^g = \mathbf{y}_\delta^g - \mathbf{a}_{3,i}^g \odot \mathbf{d}_{\delta,i}^g \tag{40}$$

$$\mathbf{y}_i^{g+1} = \frac{\mathbf{y}_{1,i}^g + \mathbf{y}_{2,i}^g + \mathbf{y}_{3,i}^g}{3} \tag{41}$$

The attack, or convergence of the method, is characterized by stopping the movement of the individuals and indicating the position of the best solution, as presented in Algorithm 4.

Algorithm 4: Gray Wolf Optimization Algorithm

Initialization.
while $g \leq g_{\max}$ **do**
  Define $\mathbf{y}_\alpha^g$, $\mathbf{y}_\beta^g$, and $\mathbf{y}_\delta^g$.
  for *each wolf* **do**
    Update the position of the wolf using (35) $-$ (41).
  end
  Update the pack of wolves;
  Evaluate the pack of wolves;
  $g \leftarrow g + 1$.
end

Section 6 will present quantitative and qualitative results obtained with the algorithms covered in this section.

5. Details of the Implementations of the Metaheuristics

For the operation of a power system with a safe operating margin when low-frequency electromechanical oscillations are present, it is necessary that the damping coefficients of these oscillatory modes present in the system be well damped for any operation point, particularly within a specified loading range. In this work, to simulate the proposed algorithms, two objective functions, F_1 and F_2, are used, which are weighted by μ_1 and μ_2. These are associated in an objective function F as can be analyzed in (42) – (44).

$$F_1 = \min_i \{ \left| \xi_i^{\text{des}} - \xi_i^{\text{calc}} \right| \} \tag{42}$$

$$F_2 = \min_i \{ \left| \omega_i^{\text{des}} - \omega_i^{\text{calc}} \right| \} \tag{43}$$

$$\text{minimize } F = \mu_1 F_1 + \mu_2 F_2 \tag{44}$$

In (42) – (44) ξ_i^{des} and ξ_i^{calc} are, respectively, the desired damping (specified in the project) and the damping calculated from the solution under evaluation, while ω_i^{des} and ω_i^{calc} are, respectively, the desired frequency (specified in the project) and the frequency calculated from the solution under evaluation for the i^{th} eigenvalue of interest. In the proposed approach, the objective is to solve a constraint satisfaction problem [29]. This means that the desired damping and frequencies are considered as restrictions of the problem and, therefore, any adjustment that provides poles within the limits specified in the Table 1 is considered as a solution to the proposed problem.

In this work, at each iteration of the optimization algorithms, the simulated pole of interest must satisfy the design conditions specified in the Table 1 and the eigenvalues of the simulated system should be allocated within a specific region in the complex plane.

Table 1: Parameters for the evaluation of the objective function.

$\xi^{\text{des}} = 0.40 \pm 20\%$ (p.u.)		$\omega^{\text{des}} = 1.40 \pm 20\%$ (Hz)	
Min.	0.32	Min.	1.12
Max.	0.48	Max.	1.68

As mentioned in Section 3, the individuals of each implemented metaheuristic are represented by vectors that contain the elements of the LQR weighting matrices, $\mathbf{Q}_c$ and $\mathbf{R}_c$, as verified in Fig. 7.

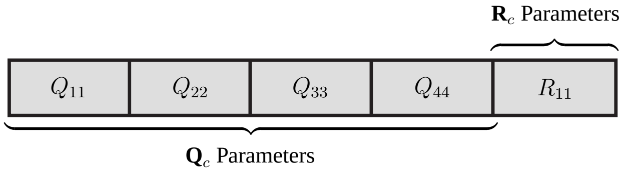

Figure 7: Representation of a solution proposal.

Once the control parameters described in Fig. 7 are determined, it is possible to determine a state feedback gain (K_{LQR}) that, after being applied to the AVR, it is possible to impose minimum damping and desired frequency (see Table 1) to the oscillatory mode present in the simulated SMIB system.

Finally, it should be mentioned that, to avoid overparameterization of the problem, it is possible to normalize matrices $\mathbf{Q}_c$ and $\mathbf{R}_c$ by imposing $R_{11} = 1$.

6. Tests and Results

When the system is simulated using the CSM in open loop and considering the data available in Table A.6 (Appendix A), a pair of complex conjugated poles $\lambda = 0.32 \pm j7.28$ is obtained, with frequency $\omega_n = 1.1593$ Hz and damping $\xi = -0.040$ p.u. Throughout the text, this case will be denoted as the *uncompensated system*. When analyzing the results obtained for the uncompensated system, it is possible to verify that the SMIB system is unstable and has a local mode, characterized by the natural undamped frequency and by the real positive part of the pole of interest. In the objective function (44), $\mu_1 = \mu_2 = 1$.

6.1. Metaheuristics Applied to the LQR Design

The parameters and implementation details of the metaheuristics are described in Table 2.

By analyzing Table 2, it can be verified that the GA uses the roulette wheel selection, crossover operator with a random chromosome cut, and the mutation occurs in each individual with the variation of 10% of the value. Regarding the DE algorithm, it is observed that it has a procedure analogous to the GA in the crossover, mutation, and elitism steps, but with adjustments of the individuals as explained in (28). The PSO algorithm follows the procedure presented in (29) – (30). Finally, the GWO uses expressions (31) – (41).

A set of 100 runs was considered for each algorithm to evaluate their effectiveness in solving the problem. The tests were conducted on a computer with a 2.20 GHz 8^{th} generation Intel® Core$^{\text{TM}}$ i3 processor and 8 GB of RAM.

Table 2: Parameters of the algorithms.

	Search Engine Structure	Algorithm Parameters	Simulation Parameters	Fitness Function
GA	Roulette selection: Crossover (1-cut): Mutation (10% of the value): Elitism:	50% probability rate 50% probability rate 10% probability rate best individual	Population size: 200 Stopping criteria: Table 1 Max. number of iter.: 100	(44)
DE	Crossover (1-cut): Mutation (10% of the value): DE function rate (28): Elitism:	50%probability rate 10% probability rate 0.3 best individual		
PSO	Equations (29) – (30)	$C_0 = 10\%$ $C_1 = 70\%$ $C_2 = 20\%$		
GWO	Equations (31) – (41)	α = 1st best individual β = 2nd and 3rd best δ = 4th – 6th best ω = the remaining ones		

The evaluation criteria used in the analysis are the number of iterations, time until convergence, and convergence error, as it can be seen in Fig. 8 and in the results shown in Table 3.

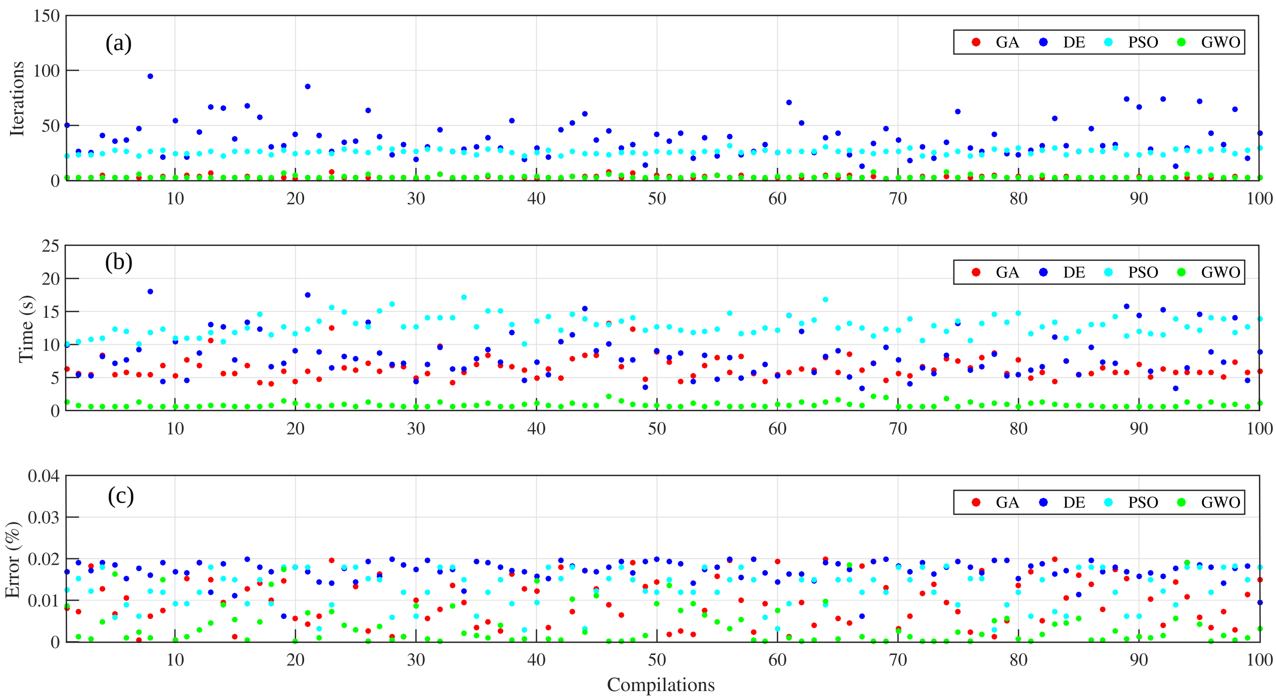

Figure 8: (a) Number of iterations, (b) time of convergence, (c) convergence error.

By analyzing the results presented in Fig. 8 and in Table 3, it can be verified that all the algorithms converged in 100% of the tests performed. When comparing the number of iterations, the GWO algorithm and the GA presented the best results. Besides that, the minimum and the maximum number of iterations required for convergence were the same in the simulations performed, however, the GWO

Table 3: Performances of the algorithms.

Algorithm		GA	DE	PSO	GWO
	Minimum	2.00	13.00	22.00	2.00
Iterations	Mean	3.70	38.61	25.61	3.56
	Maximum	8.00	95.00	32.00	8.00
	Minimum	4.07	3.37	10.10	0.65
Time (s)	Mean	6.47	8.35	12.80	0.89
	Maximum	13.17	17.94	17.18	2.12
	Minimum	2.7×10^{-4}	6.0×10^{-3}	3.0×10^{-3}	1.8×10^{-5}
Error (%)	Mean	9.80×10^{-3}	17.0×10^{-3}	12.8×10^{-3}	3.80×10^{-3}
	Maximum	19.9×10^{-3}	20.0×10^{-3}	18.1×10^{-3}	19.0×10^{-3}

algorithm converged on average with 3.56 iterations while GA converged with 3.70 iterations. When comparing the time to convergence and the convergence error, the GWO algorithm proved to be more efficient than the other approaches, converging with an average error of 3.80×10^{-3} and an average time of 0.89 seconds.

Fig. 9 shows a series of box plots with the data presented in Fig. 8 and Table 3. These plots show the statistical distribution of the data between the first quartile ($Q1^{\text{st}}$) and the third quartile ($Q3^{\text{rd}}$) (lower and upper parts of the rectangles). The second quartile ($Q2^{\text{nd}}$) or median is the red line that segments the rectangle. The lines located at the upper and lower ends of the box comprise 99% of the observed data, and the red crosses are called outliers.

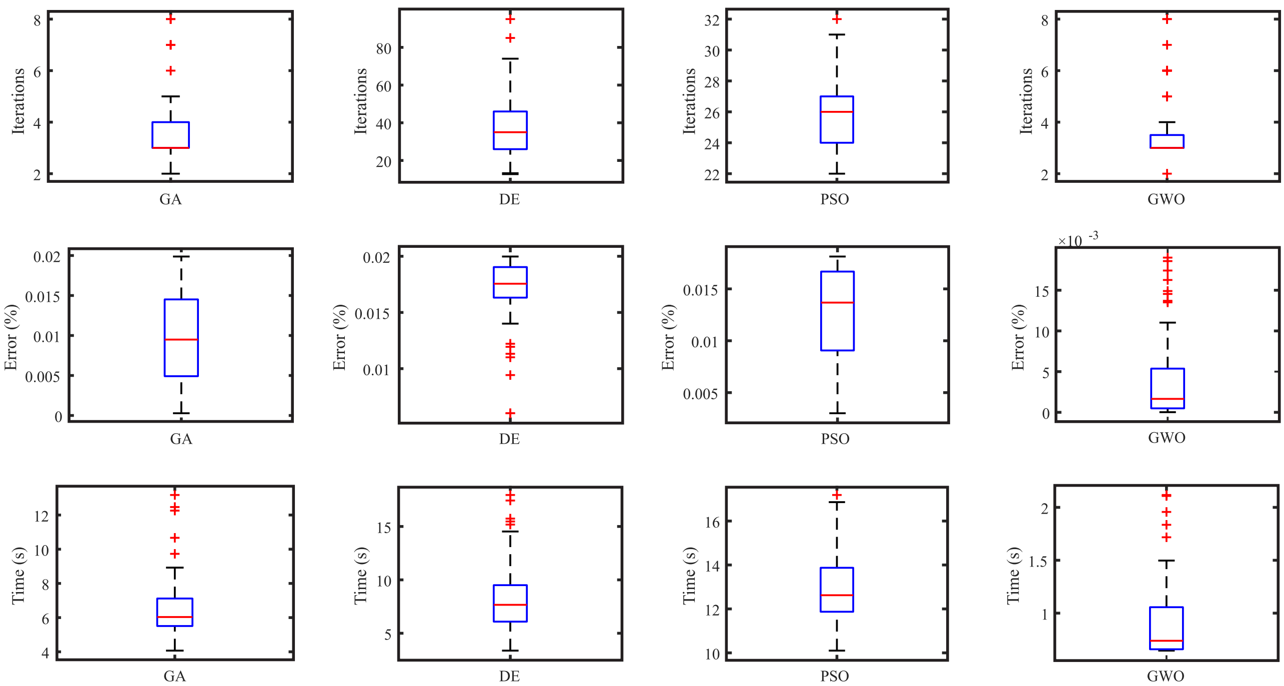

Figure 9: Box plots of the performances of the metaheuristics.

By analyzing Fig. 9 it is evident that the GWO algorithm presents a positively asymmetric arrangement of the data and the largest number of individuals outside of the normal data distribution (outliers). However, the amplitudes of the GWO algorithm plots are smaller than the others, which indicates less data dispersion. Regarding the other metaheuristics, only the GA has a more constant convergence time rate than the GWO algorithm. However, the median time for convergence of the GWO algorithm is lower than the other algorithms under study.

Fig. 10 presents a radar plot of these results. It consists of three axes that represent the execution time of the algorithms, the number of iterations, and the error.

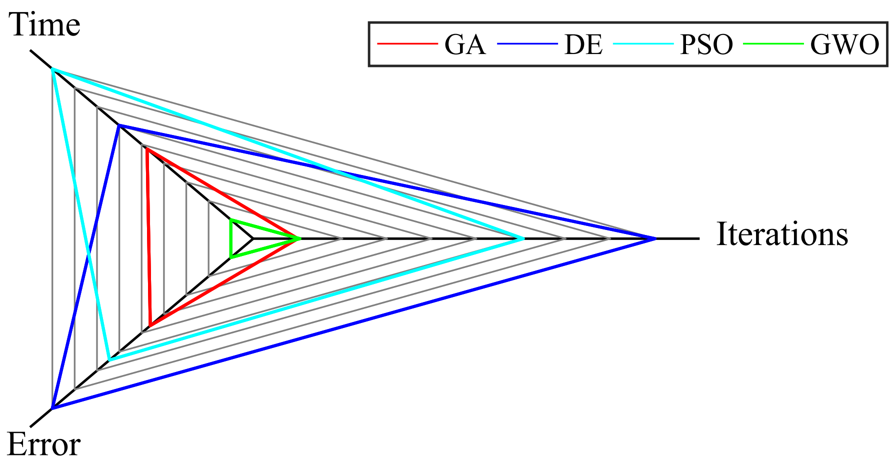

Figure 10: Radar plot of the performances of the metaheuristics.

In Fig. 10, the red, dark blue, light blue, and green curves illustrate the radar plots of the GA, DE, PSO, and GWO, respectively. Furthermore, according to the radar plot of each algorithm, it is clear that the algorithm that has the smallest convergence times, the lowest errors, and the lowest number of iterations is the GWO algorithm since its plot is the closest to the origin.

Finally, by considering the GWO algorithm and imposing $R_{11} = 1$, it was possible to find results for the problem with a similar performance to the results obtained for the GWO in this section. In this case, overparameterization of the problem can be avoided.

6.2. Evaluation of the Solutions

To verify the efficiency of the controllers, a solution from each of the previously simulated metaheuristics was selected. Their weighting matrix parameters and feedback gains are presented in (45) – (48).

$$\begin{cases} \mathbf{Q}_{\text{GA}} & = & \text{diag}([3.00 \;\; 7.00 \;\; 8.00 \;\; 0.0002]) \\ \mathbf{R}_{\text{GA}} & = & 5.00 \\ \mathbf{K}_{\text{LQR}_{\text{GA}}} & = & [59.28 \;\; -0.34 \;\; 1.43 \;\; 0.0002] \end{cases} \tag{45}$$

$$\begin{cases} \mathbf{Q}_{\text{DE}} & = & \text{diag}([1.62 \;\; 4.00 \;\; 4.00 \;\; 0.01]) \\ \mathbf{R}_{\text{DE}} & = & 6.00 \\ \mathbf{K}_{\text{LQR}_{\text{DE}}} & = & [-41.58 \;\; -0.18 \;\; 0.99 \;\; 0.0002] \end{cases} \tag{46}$$

$$\begin{cases} \mathbf{Q}_{\text{PSO}} & = & \text{diag}([2.33 \;\; 5.98 \;\; 6.35 \;\; 0.01]) \\ \mathbf{R}_{\text{PSO}} & = & 6.11 \\ \mathbf{K}_{\text{LQR}_{\text{PSO}}} & = & [-49.89 \;\; -0.26 \;\; 1.19 \;\; 0.0002] \end{cases} \tag{47}$$

$$\begin{cases} \mathbf{Q}_{\text{GWO}} & = & \text{diag}([7.19 \;\; 11.17 \;\; 14.32 \;\; 0.00]) \\ \mathbf{R}_{\text{GWO}} & = & 5.01 \\ \mathbf{K}_{\text{LQR}_{\text{GWO}}} & = & [-74.32 \;\; -0.46 \;\; 1.85 \;\; 0.0003] \end{cases} \tag{48}$$

A disturbance was simulated in $\Delta\mathbf{u}$, in the form of a sudden increase of 5% in the mechanical input power of the generator shaft. Fig. 11 shows the variation in the angular speed of the generator shaft and the response of the open-loop system, which presents an unstable behavior.

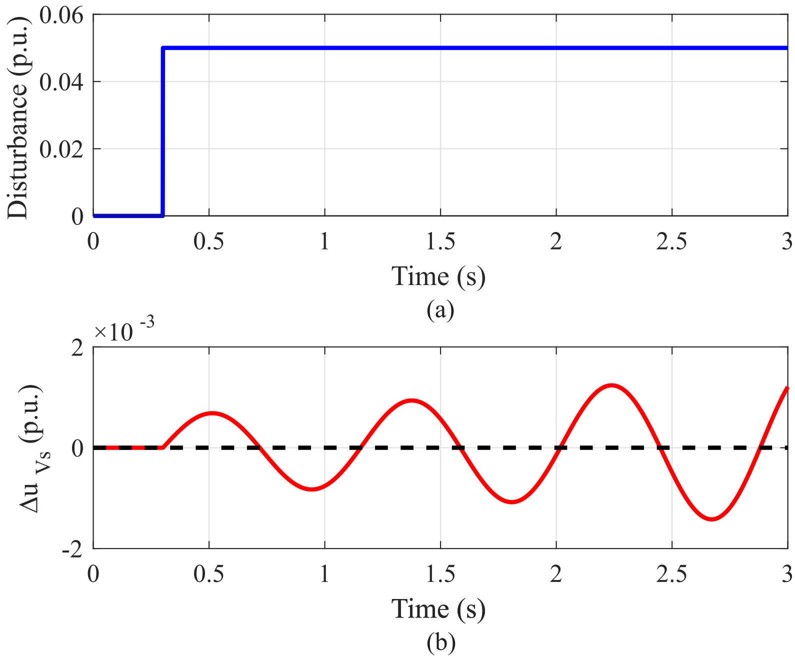

Figure 11: (a) variation in the angular speed of the generator shaft and (b) response of the open-loop system.

Fig. 12 presents the angular speed variations $\Delta\omega$ on the generator shaft and the variation of the control signal $\Delta\mathbf{u}_{\text{Vs}}$ for the closed-loop system, compensated by the LQR, for each metaheuristic.

In Fig. 12, all simulations were carried out under the same operating conditions, with the state feedback gains described in (45) $-$ (48). The numerical values presented in Fig. 12 for each pair $(\text{Time}, \Delta\omega)$ and $(\text{Time}, \Delta\mathbf{u}_{\text{Vs}})$ are, respectively, the overshoot and undershoot times for each of the LQR responses. In addition, LQR_{GA} is represented by the curve in red, LQR_{DE} by the curve in dark blue, LQR_{PSO} by the curve in light blue, and LQR_{GWO} by the curve in green. It is observed that all the algorithms achieved similar results. However, the solution of the GWO algorithm presented the lowest overshoot in $\Delta\omega$ when compared to the other responses, while the lowest undershoot in $\Delta\omega$ is achieved by the PSO algorithm.

Table 4 presents the poles of interest for both the uncompensated and compensated systems.

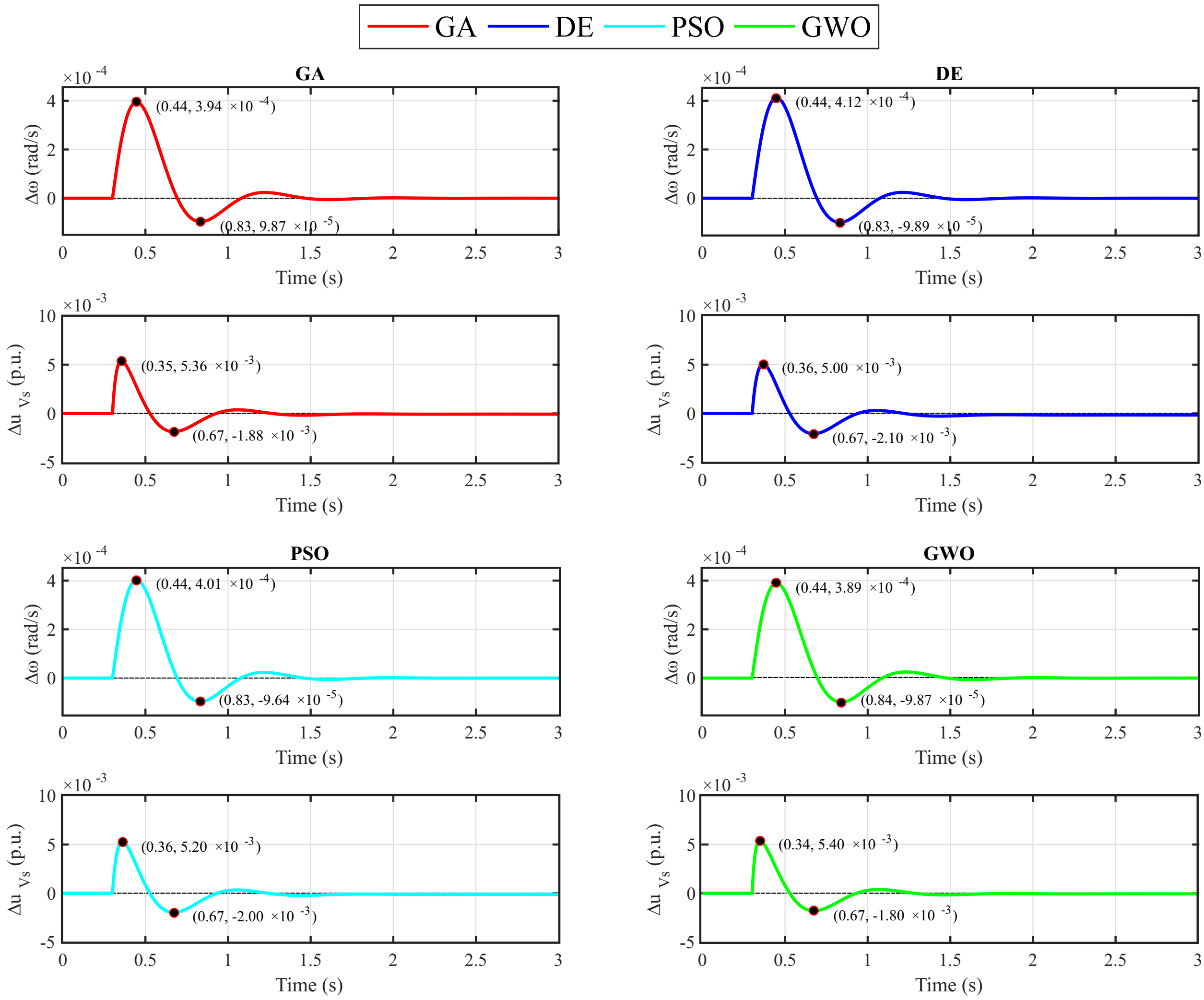

Figure 12: Variation of the angular speed of the generator shaft and control signal for the compensated system.

Table 4: Poles of interest, damping coefficients, and undamped natural frequencies of the SMIB system.

Control	$\lambda = \sigma \pm \omega$	ξ	ω_n
Open-loop	$0.32 \pm j7.28$	-0.040	1.1593
LQR-GA	$-3.51 \pm j8.03$	0.400	1.3957
LQR-DE	$-3.53 \pm j8.02$	0.403	1.3958
LQR-PSO	$-3.53 \pm j8.09$	0.400	1.4037
LQR-GWO	$-3.51 \pm j8.04$	0.400	1.3973

By analyzing Table 4, it is possible to verify that all algorithms strictly fulfilled the requirements of the project, allocating the pole of interest of the SMIB system to the region located on the left half-plane of the complex plane with frequency and damping within the specified range ($\pm 20\%$).

Table 5 presents the results of the time responses considering the integral absolute error (IAE), integral squared error (ISE), integral time-weighted absolute error (ITAE), and the integral of time-multiplied square error (ITSE) performance indices [35]. Note that the GWO algorithm has the best performance when compared to the other metaheuristics under study, with the lowest performance indices, making it clear that the LQR adjusted using the GWO algorithm has the lowest loss of responses over time.

Table 5: Performance indices.

Algorithm	GA	DE	PSO	GWO
IAE	1.2290×10^{-4}	1.2684×10^{-4}	1.2382×10^{-4}	1.2132×10^{-4}
ISE	3.0066×10^{-8}	3.2590×10^{-8}	3.0943×10^{-8}	2.9831×10^{-8}
ITAE	7.3438×10^{-5}	7.5200×10^{-5}	7.3499×10^{-5}	7.2468×10^{-5}
ITSE	1.4680×10^{-8}	1.5898×10^{-8}	1.5075×10^{-8}	1.4675×10^{-8}

7. Conclusion

This work presented a comparative analysis of the performances of four metaheuristics, namely the genetic algorithm, differential evolution algorithm, particle swarm optimization algorithm, and gray wolf optimization (GWO) algorithm for designing the parameters of a linear quadratic regulator (LQR) applied in a state feedback control over the automatic voltage regulator for damping the low-frequency electromechanical oscillations present in the single machine infinite bus (SMIB) system modeled using the current sensitivity model. The purpose of the algorithms was to provide the components of the weighting matrices and, consequently, provide the state feedback gains of the LQR.

The tests indicated the existence of a local oscillation mode in the SMIB system that caused the instability of the system. The proposal was then applied to make the system stable. The results demonstrated the effectiveness of all tested algorithms for solving the problem, with emphasis on the GWO, which, from a more detailed analysis of the results, proved to be superior to the other approaches.

In addition, an analysis was carried out considering a solution provided by each algorithm. It was evidenced that all the algorithms fulfilled the project requirements, with the damping and frequency stipulated. In this way, the simulated closed-loop system became stable with well-damped oscillations.

Future works can consider new or improved metaheuristics to solve the studied problem. Moreover, other control techniques, such as nonlinear control techniques optimized by metaheuristics and robust model predictive control design, could be used to stabilize the power system.

Appendix A. Data for the SMIB System

Table A.6 presents the data for the SMIB system.

Appendix B. Coefficients of the CSM for the SMIB System

$$K1 = \frac{V_k}{x_d^{'}} \cos(\delta - \theta) E_q^{'} + V_k^2 \cos(2\delta - 2\theta) \left(\frac{1}{x_q} - \frac{1}{x_d^{'}} \right) \tag{B.1}$$

$$K2 = \frac{V_k}{x_d^{'}} \sin(\delta - \theta) \tag{B.2}$$

$$K3 = \frac{\sin(\delta - \theta) E_q^{'}}{x_d^{'}} + V_k \sin(2\delta - 2\theta) \left(\frac{1}{x_q} - \frac{1}{x_d^{'}} \right) \tag{B.3}$$

$$K4 = -K1 \tag{B.4}$$

Table A.6: Parameters of the SMIB system.

Parameter	Value	Unit
D	0.00	kWs/kVA
H	5.00	kgm^2
ω_0	377	rad/s
T_r	1×10^{-3}	s
$T_{do}^{'}$	6.00	s
V_k	1.00	p.u.
P_l	0.50	p.u.
Q_l	0.50	p.u.
K_r	40.0	p.u.
$x_d^{'}$	0.32	p.u.
x_d	1.60	p.u.
x_q	1.55	p.u.
r_e	0.00	p.u.
x_e	0.30	p.u.

$$KA = V_k \left(\frac{x_d^{'} - x_d}{x_d^{'}}\right) \sin(\delta - \theta) \tag{B.5}$$

$$KV = \left(\frac{x_d - x_d^{'}}{x_d^{'}}\right) \cos(\delta - \theta) \tag{B.6}$$

$$R1_G = \frac{1}{x_d^{'}} \sin(\delta) \tag{B.7}$$

$$R2_G = \frac{1}{x_d^{'}} E_q^{'} \cos(\delta) + \left(\frac{1}{x_q} - \frac{1}{x_d^{'}}\right) V_k \cos(2\delta - \theta) \tag{B.8}$$

$$R3_G = -\frac{1}{x_d^{'}} \sin(\delta) \cos(\delta - \theta) + \frac{1}{x_q} \cos(\delta) \sin(\delta - \theta) \tag{B.9}$$

$$R4_G = -\frac{1}{x_d^{'}} V_k \sin(\delta) \sin(\delta - \theta) - \frac{1}{x_q} V_k \cos(\delta) \cos(\delta - \theta) \tag{B.10}$$

$$M1_G = -\frac{1}{x_d^{'}} \cos(\delta) \tag{B.11}$$

$$M2_G = -\frac{1}{x_d^{'}} E_q^{'} \sin(\delta) + \left(\frac{1}{x_q} - \frac{1}{x_d^{'}}\right) V_k \sin(2\delta - \theta) \tag{B.12}$$

$$M3_G = -\frac{1}{x_d^{'}} \cos(\delta) \cos(\delta - \theta) - \frac{1}{x_q} \sin(\delta) \sin(\delta - \theta) \tag{B.13}$$

$$M4_G = -\frac{V_k}{x_d^{'}} \cos(\delta) \sin(\delta - \theta) - \frac{V_k}{x_q} \sin(\delta) \cos(\delta - \theta) \tag{B.14}$$

$$R1 = \frac{1}{Z_e^2} \left[r_e \cos(\theta) + x_e \sin(\theta)\right] \tag{B.15}$$

$$R2 = -\frac{V_k}{Z_e^2} \left[r_e \sin(\theta) - x_e \cos(\theta)\right] \tag{B.16}$$

$$M1 = \frac{1}{Z_e^2}\left[r_e \sin(\theta) - x_e \cos(\theta)\right] \tag{B.17}$$

$$M2 = \frac{V_k}{Z_e^2}\left[r_e \cos(\theta) + x_e \sin(\theta)\right] \tag{B.18}$$

$$C1_r = -\frac{P_l \sin(\theta) - Q_l \cos(\theta)}{V_k} \tag{B.19}$$

$$C2_r = -\frac{P_l \cos(\theta) - Q_l \sin(\theta)}{V_k^2} \tag{B.20}$$

$$C3_r = \frac{\cos(\theta)}{V_k} \tag{B.21}$$

$$C4_r = \frac{\sin(\theta)}{V_k} \tag{B.22}$$

$$C1_m = -\frac{P_l \cos(\theta) - Q_l \sin(\theta)}{V_k} \tag{B.23}$$

$$C2_m = \frac{P_l \sin(\theta) - Q_l \cos(\theta)}{V_k^2} \tag{B.24}$$

$$C3_m = \frac{\sin(\theta)}{V_k} \tag{B.25}$$

$$C4_m = -\frac{\cos(\theta)}{V_k} \tag{B.26}$$

$$A_r = R4_G - R2 - C1_r \tag{B.27}$$

$$B_r = R3_G - R1 - C2_r \tag{B.28}$$

$$A_m = M4_G - M2 - C1_m \tag{B.29}$$

$$B_m = M3_G - M1 - C2_m \tag{B.30}$$

References

[1] P. Kundur, Power system stability and control, McGraw-Hill, New York, NY, USA, 1994.

[2] E. V. Fortes, L. H. Macedo, P. B. Araujo, R. Romero, A VNS algorithm for the design of supplementary damping controllers for small-signal stability analysis, International Journal of Electrical Power & Energy Systems 94 (2018) 41–56. doi:10.1016/j.ijepes.2017.06.017.

[3] S. Deckmann, V. da Costa, A power sensitivity model for electromechanical oscillation studies, IEEE Transactions on Power Systems 9 (2) (1994) 965–971. doi:10.1109/59.317649.

[4] A. Thakallapelli, R. Mehra, H. A. Mangalvedekar, Differentiation of faults from power swings and detection of high impedance faults by distance relays, in: 2013 IEEE 1st International Conference on Condition Assessment Techniques in Electrical Systems (CATCON), IEEE, 2013. doi:10.1109/catcon.2013.6737530.

[5] W. G. Heffron, R. A. Phillips, Effect of a modern amplidyne voltage regulator on underexcited operation of large turbine generators, Transactions of the American Institute of Electrical Engineers. Part III: Power Apparatus and Systems 71 (3) (1952) 692–697. doi:10.1109/aieepas.1952.4498530.

[6] E. V. Fortes, M. V. S. Costa, L. H. Macedo, P. B. Araujo, Linear quadratic regulator applied to low-frequency oscillation damping using the current sensitivity model, in: Anais do Simpósio Brasileiro de Sistemas Elétricos 2020, SBA, 2020, pp. 1–6. doi:10.48011/sbse.v1i1.2187.

[7] M. M. Rahman, A. Ahmed, M. M. H. Galib, M. Moniruzzaman, Optimal damping for generalized unified power flow controller equipped single machine infinite bus system for addressing low frequency oscillation, ISA Transactions 116 (2021) 97–112. doi:10.1016/j.isatra.2021.01.031.

[8] S. Uravakonda, V. K. Mallapu, V. R. A. Reddy, Damping enhancement for SMIB power system equipped with LQR tuned via analytical approach, Journal of The Institution of Engineers (India): Series B 101 (2020) 541–551. doi:10.1007/s40031-020-00484-3.

[9] A. Sabo, N. I. A. Wahab, M. L. Othman, M. Z. A. M. Jaffar, H. Beiranvand, Optimal design of power system stabilizer for multimachine power system using farmland fertility algorithm, International Transactions on Electrical Energy Systems 30 (12) (2020) 1–33. doi:10.1002/2050-7038.12657.

[10] M. K. Kar, S. Kumar, A. K. Singh, S. Panigrahi, A modified sine cosine algorithm with ensemble search agent updating schemes for small signal stability analysis, International Transactions on Electrical Energy Systems 31 (11) (2021) 1–29. doi:10.1002/2050-7038.13058.

[11] C.-L. Chen, Y.-Y. Hsu, Coordinated synthesis of multimachine power system stabilizer using an efficient decentralized modal control (DMC) algorithm, IEEE Power Engineering Review PER-7 (8) (1987) 32–33. doi:10.1109/mper.1987.5527040.

[12] E. L. Miotto, M. R. Covacic, Study of stability dynamic in a multimachine power system using robust controllers PSS and POD, in: 2011 Asia-Pacific Power and Energy Engineering Conference, IEEE, 2011. doi:10.1109/appeec.2011.5748844.

[13] G. Negi, A. Kumar, S. Pant, M. Ram, GWO: a review and applications, International Journal of System Assurance Engineering and Management 11 (3) (2020) 1–8. doi:10.1007/s13198-020-00995-8.

[14] J. Holland, Adaptation in natural and artificial systems: an introductory analysis with applications to biology, control, and artificial intelligence, MIT Press, Cambridge, MA, USA, 1992.

[15] J. Kennedy, R. Eberhart, Particle swarm optimization, in: Proceedings of ICNN'95 - International Conference on Neural Networks, IEEE. doi:10.1109/icnn.1995.488968.

[16] S. Mirjalili, S. M. Mirjalili, A. Lewis, Grey wolf optimizer, Advances in Engineering Software 69 (2014) 46–61. doi:10.1016/j.advengsoft.2013.12.007.

[17] R. Storn, K. Price, Differential evolution – A simple and efficient heuristic for global optimization over continuous spaces, Journal of Global Optimization 11 (4) (1997) 341–359. doi:10.1023/a:1008202821328.

[18] L. F. B. Martins, P. B. Araujo, E. V. Fortes, L. H. Macedo, Design of the PI–UPFC–POD and PSS damping controllers using an artificial bee colony algorithm, Journal of Control, Automation and Electrical Systems 28 (6) (2017) 762–773. doi:10.1007/s40313-017-0341-z.

[19] S. Abd-Elazim, E. Ali, Coordinated design of PSSs and SVC via bacteria foraging optimization algorithm in a multimachine power system, International Journal of Electrical Power & Energy Systems 41 (1) (2012) 44–53. doi:10.1016/j.ijepes.2012.02.016.

[20] B. Baadji, H. Bentarzi, A. Bakdi, Comprehensive learning bat algorithm for optimal coordinated tuning of power system stabilizers and static VAR compensator in power systems, Engineering Optimization 52 (10) (2019) 1761–1779. doi:10.1080/0305215x.2019.1677635.

[21] D. Chitara, K. R. Niazi, A. Swarnkar, N. Gupta, Cuckoo search optimization algorithm for designing of a multimachine power system stabilizer, IEEE Transactions on Industry Applications 54 (4) (2018) 3056–3065. doi:10.1109/tia.2018.2811725.

[22] E. V. Fortes, P. B. Araujo, L. H. Macedo, Coordinated tuning of the parameters of PI, PSS and POD controllers using a specialized Chu-Beasley's genetic algorithm, Electric Power Systems Research 140 (2016) 708–721. doi:10.1016/j.epsr.2016.04.019.

[23] N. A. M. Kamari, I. Musirin, A. N. Dagang, M. H. M. Zaman, PSO-based oscillatory stability assessment by using the torque coefficients for SMIB, Energies 13 (5) (2020) 1231. doi:10.3390/en13051231.

[24] H. Sun, J. Chen, J. Sun, Stochastic optimal control for sampled-data system under stochastic sampling, IET Control Theory & Applications 12 (11) (2018) 1553–1560. doi:10.1049/iet-cta.2017.1392.

[25] M. Jokarzadeh, M. Abedini, A. Seifi, Improving power system damping using a combination of optimal control theory and differential evolution algorithm, ISA Transactions 90 (2019) 169–177. doi:10.1016/j.isatra.2018.12.039.

[26] P. M. Anderson, Power system control and stability, Wiley-Interscience, Piscataway, NJ, USA, 2003.

[27] F. P. Demello, C. Concordia, Concepts of synchronous machine stability as affected by excitation control, IEEE Transactions on Power Apparatus and Systems PAS-88 (4) (1969) 316–329. doi:10.1109/TPAS.1969.292452.

[28] K. Ogata, Modern control engineering, Pearson, Upper Saddle River, NJ, USA, 2016.

[29] F. Glover, Handbook of metaheuristics, Kluwer Academic Publishers, Boston, MA, USA, 2003.

[30] S. Mirjalili, A. Lewis, The whale optimization algorithm, Advances in Engineering Software 95 (2016) 51–67. doi:10.1016/j.advengsoft.2016.01.008.

[31] S. J. Nanda, G. Panda, A survey on nature inspired metaheuristic algorithms for partitional clustering, Swarm and Evolutionary Computation 16 (2014) 1–18. doi:10.1016/j.swevo.2013.11.003.

[32] G. Rozenberg, Handbook of natural computing, Springer, Berlin, Germany, 2012. doi:10.1007/978-3-540-92910-9.

[33] S. Das, P. N. Suganthan, Differential evolution: A survey of the state-of-the-art, IEEE Transactions on Evolutionary Computation 15 (1) (2011) 4–31. doi:10.1109/tevc.2010.2059031.

[34] C. Nami, A. Harada, K. Oka, H_∞ structured controller synthesis applied to flight controller of QTW-UAV using meta-heuristic particle swarm optimization, IFAC-PapersOnLine 49 (17) (2016) 326–331. doi:10.1016/j.ifacol.2016.09.056.

[35] S. Shinners, Modern control system theory and design, Wiley-Interscience, New York, NY, USA, 1998.